Journal of Alloys and Compounds 509 (2011) 9434–9440

Contents lists available at ScienceDirect

Journal of Alloys and Compounds

journal homepage: www.elsevier.com/locate/jallcom

Magnetic and FTIR studies of $Bi_xY_{3-x}Fe_5O_{12}$ ($x = 0, 1, 2$) powders prepared by the metal organic decomposition method

Hanju Lee[a], Youngwoon Yoon[a], Hyungkeun Yoo[a], Sul A Choi[a], Kyoungchul Kim[a], Yunjung Choi[a], Harutyun Melikyan[a], Takayuki Ishibashi[b], Barry Friedman[c], Kiejin Lee[a,*]

[a] Department of Physics and Basic Science Institute for Cell Damage Control, Sogang University, Seoul 121-742, Republic of Korea
[b] Department of Materials Science and Technology, Nagaoka University of Technology, Nigata 940-2188, Japan
[c] Department of Physics, Sam Houston State University, Huntsville, TX 77341, USA

ARTICLE INFO

Article history:
Received 19 April 2011
Received in revised form 30 June 2011
Accepted 2 July 2011
Available online 23 July 2011

Keywords:
Bi–YIG
Garnet
Magnetism
Metal-organic decomposition method

ABSTRACT

The crystallization process of bismuth substituted yttrium iron garnet ($Bi_xY_{3-x}Fe_5O_{12}$; $x = 0, 1, 2$) powder prepared by the metal-organic decomposition method has been studied with various sintering temperatures. The pure garnet phase was observed for the $x = 1$ powder at 900 °C sintering temperature, whereas the $x = 0, 2$ powder showed secondary phases. The $x = 0$ powder showed a similar crystallization process to that of the solid state reaction method. For the $x = 1, 2$ powders, it is proposed that the lowering of the crystallization temperature is due to the lowered stability of the intermediate phase. The infrared spectroscopy and magnetic properties were also investigated. The pure garnet phase showed three absorption bands located at 563, 598, 655 cm^{-1} that shifted to 555, 588, 639 cm^{-1} along with an increase of bismuth concentration. The maximum values of saturation and remanence magnetization and the minimum value of coercivity were observed for the $x = 1$ powder sintered at 900 °C, which were 20.8 emu/g, 2.67 emu/g, and 31.9 Oe, respectively.

1. Introduction

Yttrium iron garnet and its derived rare-earth doped compounds have been extensively studied because of the outstanding characteristics such as a large Faraday rotation, low propagation loss, and high saturated magnetization with smaller line width in magnetic resonance [1]. In recent years, there have been many investigations of YIG and doped-YIG nanocrystals since these highly divided materials can be used in Faraday magneto-optical devices for telecommunications, high-density magnetic or magneto optical information storage, and so on [2]. In particular, bismuth doped yttrium iron garnet (Bi–YIG) has attracted much attention due to the high transmittance and huge Faraday rotation for visible wavelengths [3].

The conventional solid state reaction method often requires prolonged grinding and high sintering temperature which yields large particles and poor chemical homogeneity [2]. To overcome these disadvantages, there have been many studies using various chemical solution decomposition (CSD) methods, such as the sol–gel method [4], hydrothermal synthesis [5], and the coprecipitation method [2]. Indeed, recent studies based on the CSD methods showed a successful preparation of garnet nanocrystals with low sintering temperature [2,4–6].

The CSD methods have a unique advantage of homogeneity and controllability of composition along with the capability of large area deposition in combination with easy and simple processing. Among these methods, since the metal-organic decomposition (MOD) method uses chemically stable solvents, such as carboxylic acid, it could be a promising technique keeping the above advantages along with chemical stability.

Despite these advantages, the MOD method has been less studied than other CSD methods. In the CSD method, crystallization kinetics and physical properties are strongly dependent on the types of ligand, kinds of solution, and heating schedule [7]. To prepare high quality material, it is necessary to understand the synthesis process in crystallization. In the present study, we investigated the synthesis process and crystallization behavior in the MOD method for YIG and Bi–YIG powder with different doping concentrations.

2. Experimental details

MOD solutions of $Bi_xY_{3-x}Fe_5O_{12}$ ($x = 0, 1, 2$) were purchased from Kojundo Chemical Laboratory. The chemical composition of the MOD solution was selected to have ratios of Bi:Y:Fe of 0:3:5, 1:2:5, 2:1:5, respectively. Each element was synthesized to organo-metallic complexes from carboxylic acids with carbon numbers from 3 to 20 by a reaction with rosin, in organic solvents such as esters. The detailed synthesis is presented in reference [3].

* Corresponding author. Tel.: +82 2 715 8425; fax: +82 2 715 8429.
E-mail address: klee@sogang.ac.kr (K. Lee).

0925-8388/$ – see front matter © 2011 Elsevier B.V. All rights reserved.
doi:10.1016/j.jallcom.2011.07.005

To prepare the powders, each solution was dried at 150 °C for one week, and was ground by a mortar. To investigate the crystallization process, each powder was sintered at 400–1200 °C, and examined by powder X-ray diffraction (XRD) and Fourier transform infrared spectroscopy (FTIR). Magnetic properties were studied by a vibrating sample magnetometer (VSM).

3. Results and discussion

3.1. XRD results of the x = 0 powder

Fig. 1(A) and (B) shows the XRD pattern of undoped YIG powders sintered at 400–1200 °C. The XRD pattern of the powder sintered at 400 °C shows a strong maghemite (γ-Fe_2O_3) phase [8] with an additional broad peak near 29° (marked as '*') and a small peak near 33° (marked as '+'). When the sintering temperature was increased up to 500 °C, the diffraction peaks became stronger and a new peak near 48° (marked as '@') and 52° (marked as '#') appeared. The two broad peaks near 29° and 48° can be assigned to a yttrium oxide (Y_2O_3) [9], and the broadness suggests that yttrium oxide consists of an amorphous phase or fine particles. The peak near 33° (marked as '+') can be assigned to the hexagonal or orthombic yttrium iron oxide (h-$YFeO_3$, o-$YFeO_3$) or the hematite (α-Fe_2O_3) phase, but from the relation with a peak near 52°, indicates it should be assigned to the h-$YFeO_3$ phase [10]. As the sintering temperature increased, the diffraction peaks of the Y_2O_3 and h-$YFeO_3$ phases became stronger. Sintered powder at 700 °C showed a similar diffraction pattern to the patterns of the powders sintered at 400–600 °C. When the sintering temperature increased up to 800–1100 °C (Fig. 1(B)), the diffraction pattern of the powders is drastically changed. The maghemite phase and broad peaks of yttrium oxide disappeared and o-$YFeO_3$ [10] appeared as a major phase along with a weak garnet phase [11]. The peak related to the h-$YFeO_3$ located near 52° remained at 800 °C but disappeared at higher sintering temperature (900–1200 °C). The garnet phase peaks became stronger with increasing of sintering temperature, but the orthoferrite phase became weaker and remained up to 1300 °C (the XRD pattern of 1300 °C showed a similar pattern, so it is not presented). The remaining YFO phases may be due to insufficient sintering time or chemical inhomogeneity caused by decomposition of the organic parts. The appearance and crystallization temperature of the garnet phase was similar to other preparation methods [12–14].

For the powders sintered at high temperature (T > 800 °C), the observed phases and appearance and crystallization temperature of garnet was similar to that of the solid state reaction (SSR) method. This suggests that the crystallization process is similar to the SSR method and described by the following equations:

$$Y_2O_3 + Fe_2O_3 \rightarrow 2YFeO_3; \qquad \text{at } 800\text{–}1200\,^\circ\text{C},$$

$$3YFeO_3 + Fe_2O_3 \rightarrow Y_3Fe_5O_{12}; \qquad \text{at } 1000\text{–}1300\,^\circ\text{C}.$$

and means that the crystallization process does not depend on chemical reactions of organic ligands or its influence on the crystallization process is very limited. However, at lower sintering temperature, the sintered powders showed two metastable phases: γ-Fe_2O_3 and h-$YFeO_3$, and this suggests that the crystallization process is related to the decomposition process of the initial organic compounds.

For the powders sintered at lower temperature (T < 700 °C), there was an interesting phase, h-$YFeO_3$, which is suggested as a metastable phase in the Fe_2O_3-Y_2O_3 system, and at high temperature (~860 °C), the h-$YFeO_3$ phase is transformed to other two stable phase: o-$YFeO_3$ (orthohombic, perovskite structure) or $Y_3Fe_5O_{12}$ (cubic, garnet structure) [11,15,16]. For the formation of the h-$YFeO_3$ phase in selective self-propagating combustion synthesis [10], the authors reported that the lowering of flame temperature results in the preferred formation of h-$YFeO_3$. In our experiment, the precursors had a large carbon chain and were dissolved in non-interacting solvent, therefore, the formation of metal oxides occurs by thermal decomposition of the organic part. When the thermal decomposition of the reactants happens, they are very unstable as compared to the final product. The crystal growth of the product is directly associated with the decomposition process so that the metastable phase would be formed preferentially due to a large driving force provided by the reaction [15].

It is worthwhile to note the existence of the γ-Fe_2O_3 phase at relatively high sintering temperature. Maghemite, the ferromangetic cubic form, is a metastable polymorph of the Fe_2O_3 system and is transformed to stable hematite (α-Fe_2O_3) around 300–400 °C. It was reported that the transition temperature is increased up to 700 °C when the nanocrystalline maghemite is supported on a silica matrix [17]. The authors suggested that the interaction between iron atoms and silica matrix stabilizes the maghemite phase so that the transition temperature is increased. Similar result have been reported for the Y_2O_3 doped γ-Fe_2O_3 prepared by a sol–gel method that showed an increase of the transformation temperature up to 775 °C with 12.4 mol% yttrium concentration [8]. In our experiment, the existence of the maghemite phase up to 700 °C may be explained by the same reason: Y_2O_3 would stabilize the maghemite phase by interaction with iron ions.

3.2. XRD results of x = 1,2 powder

Fig. 2(A) and (B) shows the XRD pattern of $Bi_xY_{3-x}Fe_5O_{12}$ (x = 1, 2) powders sintered at 400–900 °C. At 400 °C, the pattern of the x = 1 powder showed two phases: a major phase, β-Bi_2O_3 [18], and a minor phase, γ-Fe_2O_3. In the case of x = 2, there are three phases: β-Bi_2O_3, tetragonal $Y_nBi_{1-n}FeO_3$ (t-YBFO) [19] and γ-Fe_2O_3, and the t-YBFO phase was stronger than the γ-Fe_2O_3 phase. When the sintering temperature was increased up to 500 °C, for the x = 1 case, several broad peaks corresponding to the t-YBFO and Y_2O_3 phases appeared and the β-Bi_2O_3 phase peaks are buried in those peaks. However, for the x = 2 powder, the β-Bi_2O_3 phase peaks remained distinguishable and weaker than the t-YBFO phase. When the sintering temperature was increased up to 600 °C, the β-Bi_2O_3 phase completely disappeared for both x = 1, 2, and this temperature is similar to the transition temperature from the β-Bi_2O_3 to the α-Bi_2O_3 or the δ-Bi_2O_3 phase (497–600 °C) [20]. We note that the YBFO phase showed tetragonal structure rather than rhombohedral structure. It has been reported that the structural transition from rhombohedral to tetragonal phase occurs when the yttrium concentration is greater than 0.15 [19].

When the sintering temperature was 700 °C, the garnet phase appeared in both samples, and the appearance temperature was comparable to other preparation methods [11,21]. For the x = 1 powder, the diffraction pattern showed a orthohombic structure (o-YBFO) which usually appears when $BiFeO_3$ is doped by a lanthanide element [22]. Lattice parameters derived from the XRD pattern were: a = 5.3909 Å, b = 5.6742 Å, c = 7.6892 Å, and these were comparable to reported values of $BiFeO_3$ doped by 30 mol% Gd (GdBFO): a = 5.4206 Å, b = 5.6329 Å, c = 7.7889 Å [23]. Because the ionic radius of Bi^{3+} is larger than that of Y^{3+}, it is expected that the lattice parameter of o-YBFO is larger than that of o-YFO. The smaller lattice parameters of the x = 0 powder (a = 5.3505, b = 5.6315, c = 7.6753) is consistent with this suggestion, but the difference of lattice parameters was not isotropic: Δa, $\Delta b \approx 0.04$ Å and $\Delta c \approx 0.01$ Å, indicating a distortion of the lattice geometry. Similar behavior was reported in yttrium–lanthanum orthoferrite, which showed an anisotropic contraction when the lanthanum ion was substituted by yttrium which has a smaller ionic radius than lanthanum [24]. The XRD pattern of the x = 2 powder showed a strong t-YBFO phase with a weak garnet phase. Lattice parameters of the t-YBFO phase

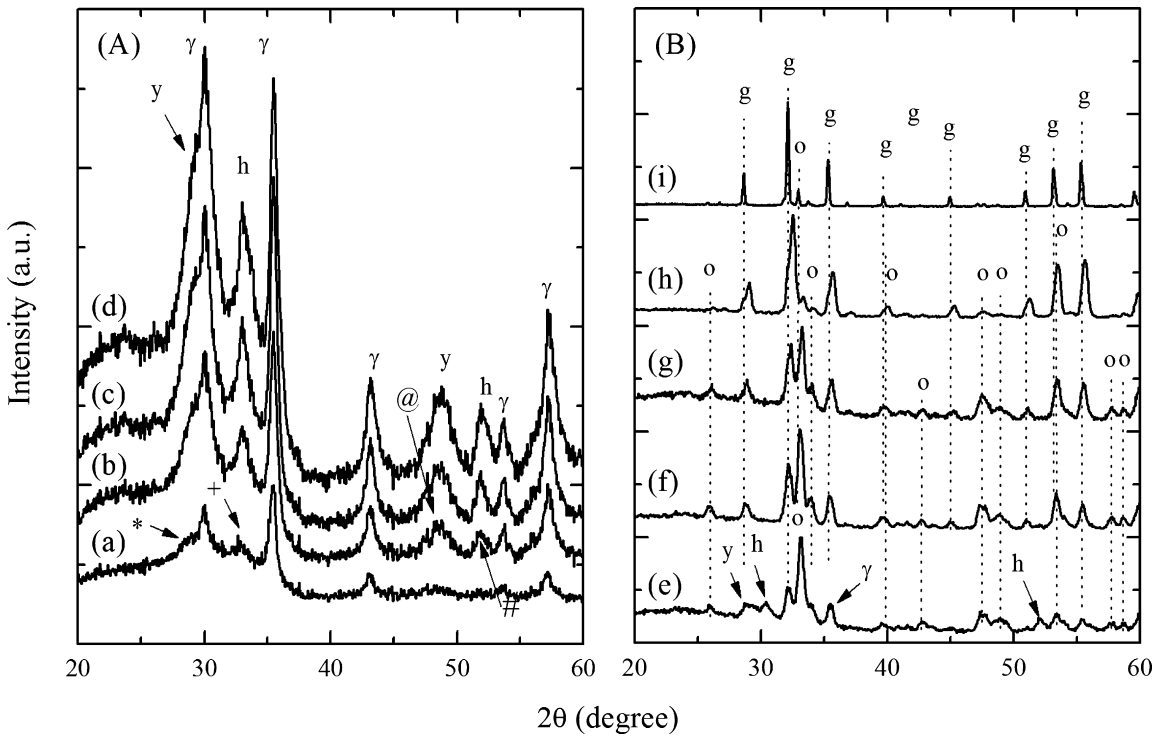

Fig. 1. XRD pattern of the $x = 0$ powder sintered at 400–700 °C (A) and 800–1200 °C (B): (a) 400 °C, (b) 500 °C, (c) 600 °C, (d) 700 °C, (e) 800 °C, (f) 900 °C, (g) 1000 °C, (h) 1100 °C, and (i) 1200 °C. Assignment of diffraction peaks are indicated as following: g: garnet, o: o-$YFeO_3$, h: h-$YFeO_3$, γ: γ-Fe_2O_3, y: Y_2O_3.

calculated from the XRD pattern were: $a = 5.5457$ Å, $c = 12.5893$ Å, and are comparable to that of the reference values when the yttrium concentration was 0.15: $a = 5.5619$ Å, $c = 12.5305$ Å [19].

Increasing the sintering temperature to 800 °C, the intensity of diffraction peaks of the garnet phase were comparable to the YBFO phase in both powders, and at 900 °C, the powder $x = 1$ showed only the garnet phase diffraction pattern whereas the powder $x = 2$ showed a weak $BiFeO_3$ phase along with another secondary phase, $Bi_2Fe_4O_9$, which usually appears as a secondary phase for $BiFeO_3$ and Bi–YIG when bismuth has excessive composition [21]. Lattice parameters of the garnet phase for the $x = 1$, 2 powder were 12.44, 12.48 Å, respectively, larger than that of the $x = 0$ powder

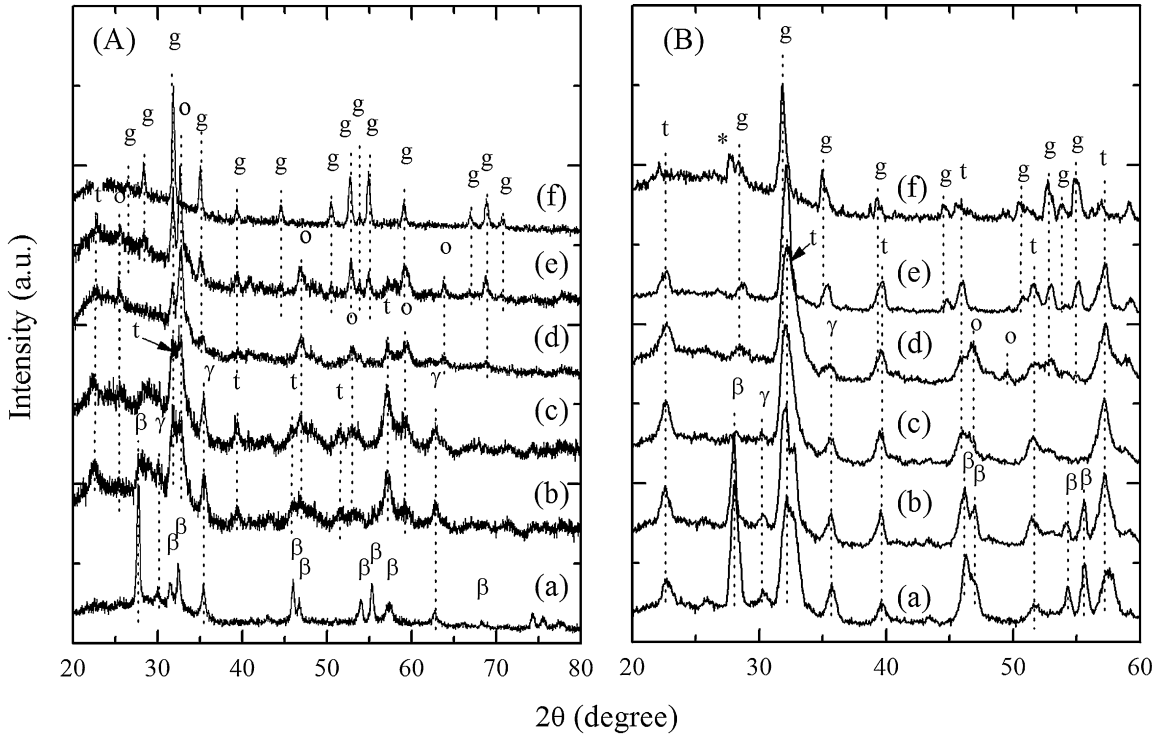

Fig. 2. XRD pattern of the $x = 1$ (A) and $x = 2$ (B) powders sintered at 400–900 °C: (a) 400 °C, (b) 500 °C, (c) 600 °C, (d) 700 °C, (e) 800 °C, and (f) 900 °C. Assignment of diffraction peaks are indicated as following: g: garnet, o: o-YBFO, t: t-YBFO, γ: γ-Fe_2O_3, β: β-Bi_2O_3.

(12.3286 Å) and the reported value (12.376 Å) for pure YIG [25]. This increase is due to the substitution of small Y^{+3} by big Bi^{+3}, and the larger lattice parameter of garnet in $x = 2$ powder indicates that the phase is more highly doped by bismuth. The lattice parameter of the $x = 1$ powder was similar to reported values, but for the $x = 2$ powder, the lattice parameter was similar to that of $x = 1.8$. It is known that the bismuth concentration cannot exceed 1.8 in the garnet phase because of its large lattice constant, and this is consistent with our result.

It is worthwhile to compare the difference of phase formation between the $x = 0$ and the $x = 1, 2$ powders. For the $x = 0$ powder, the γ-Fe_2O_3 phase combined with Y_2O_3 is more stable than the o-$YFeO_3$ phase at 400 °C, then at 700 °C, the γ-Fe_2O_3 phase is slowly decomposed. For the $x = 1$ powder, the t-YBFO phase already appeared at lower temperature ($T > 500$ °C), and as we increase the sintering temperature, the t-YBFO phase is transformed to o-YBFO. At 700 °C, a rapid increase of the o-YBFO phase peak together with a decrease of the Y_2O_3 phase peak is observed. The rapid increase of the o-YBFO phase with the disappearance of the Y_2O_3 suggests that the structural transition induced by a reaction with Y_2O_3 is described by the following mechanism:

$$\gamma\text{-}Fe_2O_3 + \beta\text{-}Bi_2O_3 \rightarrow 2BiFeO_3[\text{rhombohedral}];$$

$$2(1-n)BiFeO_3[\text{rhombohedral}] + nY_2O_3 + nFe_2O_3 \rightarrow 2Y_nBi_{1-n}FeO_3[\text{tetragonal}]; \quad \text{at } T < 600\,^{\circ}\text{C}, n < 0.1$$

$$2(1-\text{m})Y_nBi_{1-n}FeO_3[\text{tetragonal}] + mY_2O_3 + \text{m}Fe_2O_3 \rightarrow 2Y_{n+m}Bi_{1-n-m}FeO_3[\text{orthohombic}]; \quad at\ T = 700\,^{\circ}\text{C}\ n + m > 0.3.$$

For the crystallization of the Bi–YIG phase, it is known that the crystallization temperature is lowered with an increasing concentration of bismuth [26,27]. Although this phenomena has been well known for a long time, there have been few papers dealing with the lowering of the crystallization temperature. In the SSR method, it was reported that the lowering of the crystallization temperature of garnet and hexaferrite [27] is due to the existence of a liquid phase of Bi_2O_3. The authors suggest that the liquid phase enhances the ion diffusion so that the crystallization temperature is lowered. However, in our study, because the bismuth does not exist as a oxide but as a organic compound, the crystallization process is different from the SSR method. The appearance of t, o-YBFO phase at relatively lower sintering temperature ($T < 500$ °C) suggests that when the garnet phase is crystallized, the bismuth does not exist as a Bi_2O_3 phase but as a t, o-YBFO phase. Therefore, it is plausible that the crystallization of the garnet phase of Bi–YIG powder ($x = 1$, 2) is through the intermediate $Y_nBi_{1-n}FeO_3$ phase:

$$3Y_nBi_{1-n}FeO_3 + Fe_2O_3 \rightarrow Y_{3n}Bi_{3-3n}Fe_5O_{12}; \quad at\ T = 700\,^{\circ}\text{C}, n < 1.$$

In the study of the thermodynamic stability of $BiFeO_3$ and related Bi-based perovskites [28], the authors show that $BiFeO_3$ follows a trend of perovskites (ABO_3), and a substitution on the A site with a larger or more basic cation stabilizes the preovskites phase. Compared to Bi, Y has a smaller ionc radius but is a more basic cation. This suggests that the substitution of Y for Bi would stabilize the BFO phase. It was reported that when the concentration of yttrium was 0.1, the $BiFeO_3$ single phase was observed, but when the concentration was increased up to 0.3, secondary phases like a garnet phase were observed [19]. This result suggests that despite that yttrium is a more basic cation than bismuth, the $BiFeO_3$ phase becomes unstable to the garnet phase when the concentration of yttrium is increased up to 0.3. The lowering of crystallization temperature of Bi substituted YIG may be related to this result. The $x = 1$, 2 powders sintered at lower temperature ($T < 600$ °C) showed the Y doped BFO phase, and when the sintering temperature increased up to 700 °C, the garnet phase appeared and the diffraction peaks became stronger while the YBFO phase became weaker. This suggests that at high temperature ($T > 700$ °C), the YBFO phase became unstable to the garnet phase so the preferred crystallization to the garnet phase occurs.

3.3. FTIR studies

Fig. 3(A) shows FTIR transmittance spectra of $x = 0$ powders sintered at 400–1200 °C between 400 and 800 cm^{-1}. Sintered powders at 400–700 °C showed three absorption peak at 558, 635, 693 cm^{-1}, and these bands can be assigned to Fe–O vibration of γ-Fe_2O_3 [29]. When the sintering temperature increased up to 800 °C, absorption bands of γ-Fe_2O_3 disappeared and the band located at 558 cm^{-1} shifted to 563 cm^{-1}, which correspond to the Fe–O stretching mode of the perovskite system [19], and a new absorption band appeared at 598 cm^{-1}. The sintered powder at 1200 °C showed three absorption bands at 563, 598, 655 cm^{-1}, and these bands can be assigned to the asymmetric stretching of the tetrahedron Fe–O bond of YIG [30]. Fig. 3(B) and (C) shows FTIR transmittance spectra of $x = 1$, 2 powders sintered at 400–900 °C between 400 and 800 cm^{-1}, respectively. The two powders ($x = 1$, 2) sintered at 400–600 °C showed three absorption bands of γ-Fe_2O_3 similar to the $x = 0$ powder. Absorption bands of γ-Fe_2O_3 of $x = 1$, 2 powders disappeared at 700 °C, and new absorption band related to the perovskite appeared at 556 cm^{-1} for $x = 1$, and 551 cm^{-1} for $x = 2$ powder. At the higher sintering temperature (800–900 °C), three absorption bands appeared at 558, 595, 646 cm^{-1} for the $x = 1$ powder, and at 555, 588, 639 cm^{-1}, for the $x = 2$ powder. The disappearance and appearance temperature of the absorption bands related to orthoferrite and garnet were consistent with the XRD results.

The absorption bands corresponding to garnet and perovskite showed a tendency to shift to lower frequency with increase of the bismuth concentration. Fig. 4(A) and (B) shows the FTIR transmittance spectra corresponding to the perovskite phase and the garnet phase. For the band shift of the garnet phase, it was reported that that the absorption bands have linear behavior with the unit cell volume, and when the rare-earth ion is substituted by a larger rare earth element, the band is shifted to lower frequency due to the decrease of the Fe–O bond strength [30]. The band shift of YFO to lower frequency along with the bismuth concentration indicates that the force constant of the Fe^{3+}–O^{-2} bond changes. Similar result has been reported for $Dy_xBi_{1-x}FeO_3$ solid solutions [31]. The authors reported that the absorption frequencies are sensitive to the structure of $Dy_xBi_{1-x}FeO_3$ rather than the mass of the vibrating ions. These results are consistent with our observation in the XRD experiment that showed a structural transition as a function of bismuth concentration. However, more detailed studies are required to further confirm this conclusion.

3.4. Magnetic properties

Fig. 5(A) and (B) shows the sintering temperature dependence of M_S and H_C and M_R. The saturation magnetizations (M_S) of the powders sintered at 400–600 °C were 10∼17 emu/g, and the maximum value observed from the powder sintered at 500 °C, is 17.327 emu/g. From the XRD result, because only the γ-Fe_2O_3 phase has a strong ferrimagnetic property among the observed phases at those temperatures, the magnetic behavior of sintered powders at 400–600 °C would strongly depend on the γ-Fe_2O_3 phase. The M_S values were comparable to the value of γ-Fe_2O_3 nanoparticle in

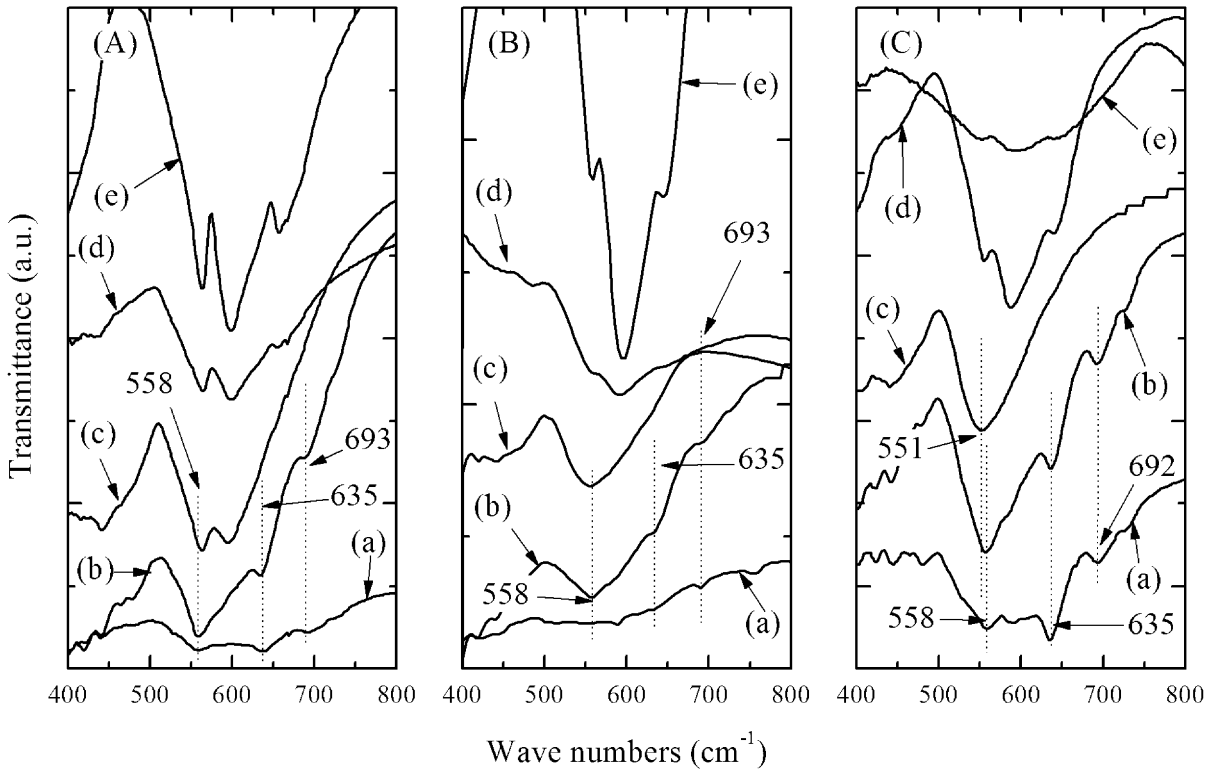

Fig. 3. FTIR transmittance spectra of the powders: (A) for $x = 0$ powder sintered at (a) 400 °C, (b) 700 °C, (c) 800 °C, (d) 900 °C, and (e) 1200 °C; (B) for $x = 1$ and (C) for $x = 2$ powders sintered at (a) 400 °C, (b) 600 °C, (c) 700 °C, (d) 800 °C, and (e) 900 °C.

a silica matrix [32]. The low coercivity (H_C) and remanence magnetization (M_R), and un-saturated magnetization at high magnetic field suggests that γ-Fe_2O_3 exhibits weak and soft ferromagnetic and superparamagnetic behaviors [33]. The particle size was calculated by Scherrer's equation, and estimated to be about 15.4 nm, and this value is slightly larger than that of superparamagnetic γ-Fe_2O_3 nanoparticles [32]. In the range of 500–600 °C, the M_S and M_R decreased whereas the H_C showed an increase. The decrease of

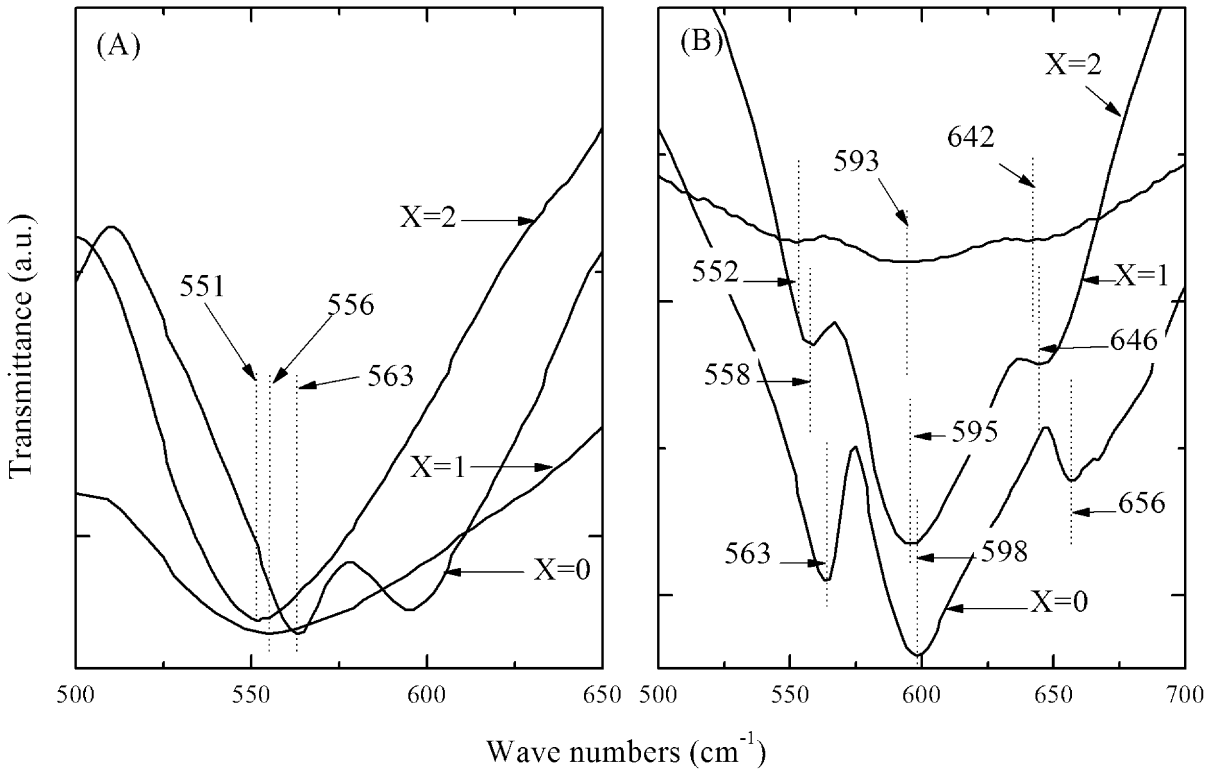

Fig. 4. FTIR transmittance spectra of sintered powder: (A) sintered at 800 °C for $x = 0$, and 700 °C for $x = 1, 2$, (B) sintered at 1200 °C for $x = 0$, and 900 °C for $x = 1, 2$.

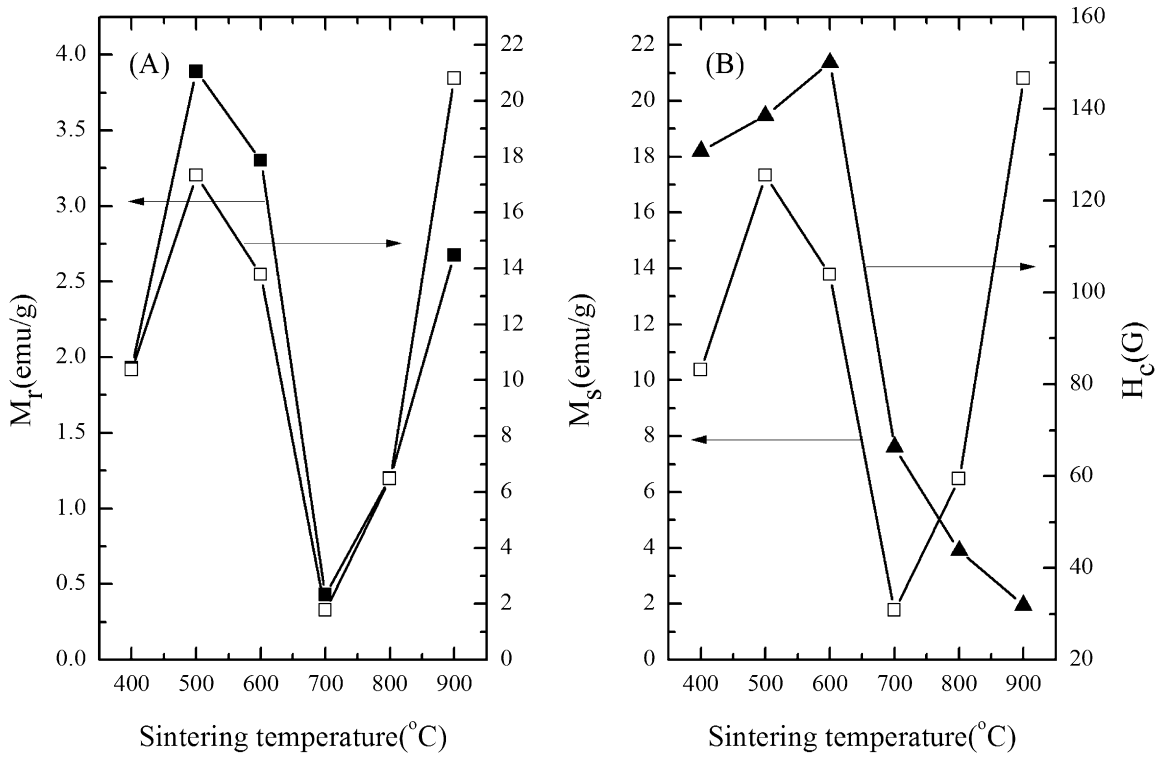

Fig. 5. Variation of saturation magnetization (M_S), coercivity (H_C), and remanence magnetization (M_R) of $x = 1$ powders as a function of sintering temperature.

M_S and M_R would be due to the YBFO phase formation showing a weak ferrimagnetic property, wheares the increase of H_C suggests an increase of particle size [34].

These three values drastically decreased at 700 °C, and as an increase of sintering temperature, the M_S and M_R increased whereas the H_C decreased continuously. From the XRD result, the magnetic property of the powder at this sintering temperature range would strongly depend on the YBFO and garnet phase. For the magnetic property of $BiFeO_3$, it is well known that the magnetic property originates from G-type anti-ferromagnetism at room temperature and shows weak ferrimagnetic behavior [19,35]. In the study of size dependent magnetic properties of $BiFeO_3$ nanoparticles [35], it was reported that the M_S and H_C increase as the particle size decreases. The reported values for 14 nm $BiFeO_3$ nanoparticles were: $M_S = 1.55$ emu/g, $H_C = 58$ Oe, and these are comparable to the measured values of the sintered powder at 700 °C: $M_S = 1.779$ emu/g, $H_C = 66.351$ Oe. The particle size of the YBFO phase estimated by Scherrer's equation was 13.9 nm and it is also comparable to the reference value. However, for M_R, the difference between the measured value (0.429 emu/g) and reference value (0.032 emu/g) was an order of magnitude. This deviation suggests that the garnet phase contributes to the magnetic properties of the powder. With the increase of sintering temperature from 700 °C up to 900 °C, the M_S and M_R increased, whereas the H_C decreased. The maximum value of M_S and M_R and the minimum of H_C observed at 900 °C was 20.8 emu/g and 2.67 emu/g, 31.9 Oe, respectively, and they are comparable to the reported values [26].

Fig. 6 shows magnetic hysteresis curves of the powders sintered at 900 °C for $x = 1, 2$, and sintered at 1200 °C for $x = 0$. The M_S of the $x = 0$ powder was 20.5 emu/g and this value was slightly smaller than that of the $x = 1$ powder. It may be due to the existence of a secondary phase of $x = 0$ powder, and it is known that the substitution of bismuth enhances the superexchange coupling between the ferric ions and results in a increase of the magnetic moment [11]. These two factors would lead to a larger magnetic moment of the $x = 1$ powder. The M_S of $x = 2$ powder was 9.13 emu/g, and this value was much smaller than that of $x = 0, 1$ powders. This may be due to the poor crystallinity and existence of a secondary phase. It is known that when the bismuth concentration is as high as 1.8, Bi–YIG cannot be grown because of its large lattice constant. The XRD pattern of $x = 2$ powder sintered at 900 °C showed stronger secondary phases and a broader garnet phase peak than the $x = 0$, 1 powder. Thus, it is plausible that the poor crystallinity and secondary phases leads to the decrease of the magnetic moment of the $x = 2$ powder.

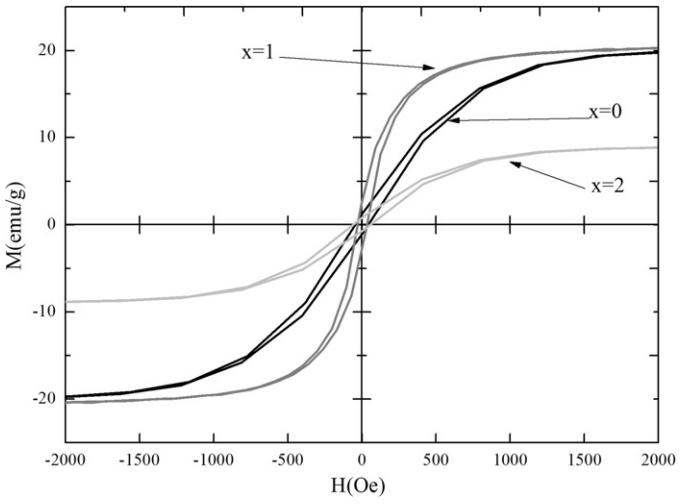

Fig. 6. Room temperature hysteresis loops of powders sintered at 900 °C for $x = 1, 2$ and at 1200 °C for $x = 0$ powder.

4. Conclusions

The crystallization of $Bi_xY_{3-x}Fe_5O_{12}$ ($x = 0, 1, 2$) powder prepared by the MOD method has been studied. In the lower temperature region (400–700 °C), the XRD patterns of $x = 0$ powder showed a strong maghemite phase, whereas the XRD patterns of $x = 1, 2$ powders showed o, t-YBFO as a major phase. At higher temperatures, the $x = 0$ powder showed similar crystallization process to the SSR method (800–1200 °C), but for the $x = 1, 2$ powders, it was proposed that the crystallization to the garnet phase is through an intermediate phase, and suggested that the lowering of the crystallization temperature is due to the lowered stability of the YBFO phase compared to the YFO phase. The pure garnet phase was observed at 900 °C for the $x = 1$ powder, but for the $x = 2$ powder, secondary phases were observed with the garnet phase. FTIR and magnetic properties of the garnet phase were also examined. The IR absorption band shift according to bismuth concentration was observed, and it was suggested that the shift would be due to the structural distortion induced by difference of ionic radius of yttrium and bismuth. The magnetic properties of the garnet phase of the $x = 0$, 1 powders were similar to the reported values, but for the $x = 2$ powder, M_S was decreased because of poor crystallinity and existence of secondary phases.

Acknowledgements

This work was supported by a Sogang University Special Research Grant (2011), Basic Science Research Program through the National Research Foundation of Korea Grant (2011-0004688), and Priority Research Centers Program through the National Research Foundation of Korea (2010-0028297).

References

[1] X.-W. Zhang, J. Cryst. Growth 310 (2008) 3235–3239.
[2] W. Zhang, C. Guo, R. Ji, C. Fang, Y. Zeng, Mater. Chem. Phys. 125 (2011) 646–651.
[3] T. Ishibashi, A. Mizusama, M. Nagai, S. Shimizu, K. Sato, N. Togashi, T. Mogi, M. Houchido, H. Sano, K. Kuriyama, J. Appl. Phys. 97 (2005) 013516.
[4] N. Nasir, N. Yahya, M. Kashif, H. Daud, M.N. Akhtar, H.M. Zaid, A. Shafie, L.C. Teng, J. Nanosci. Nanotechnol. 11 (2011) 2551–2554.
[5] L. Guo, K. Huang, Y. Chen, G. Li, L. Yuan, W. Peng, H. Yuan, S. Feng, J. Solid State Chem. 184 (2011) 1048–1053.
[6] L. Yu, L. Zeng, C. Lu, W. Zhang, G. Xu, Mater. Charact. 62 (2011) 378–381.
[7] R.W. Schwartz, T. Schnelle, R. Waser, C. R. Chim. 7 (2004) 433–461.
[8] S. Tao, X. Liu, X. Chu, Y. Shen, Sens. Actuators B 61 (1999) 33–38.
[9] J. Lee, Y. Tak, J. Ind. Eng. Chem. 5 (1999) 139–142.
[10] L. Wu, C.Y. Jimmy, L. Zhang, X. Wang, S. Li, J. Solid State Chem. 177 (2004) 3666–3674.
[11] T. Kim, S. Nasu, M. Shima, J. Nanopart. Res. 9 (2007) 737–743.
[12] A. Sztaniszláv, E. Sterk, L. Fetter, M. Farkas-Jahnke, J. Lábár, J. Magn. Magn. Mater. 41 (1984) 75–78.
[13] Y.S. Ahn, M.H. Han, J. Mater. Sci. 31 (1996) 4233–4240.
[14] C.D. Veitch, J. Mater. Sci. 26 (1991) 6527–6532.
[15] M. Inoue, T. Nishikawa, T. Nakamura, T. Inui, J. Am. Ceram. Soc 80 (1997) 2157–2160.
[16] O. Yamaguchi, H. Takemura, M. Yamashita, A. Hayashida, J. Electrochem. Soc. 138 (1991) 1492–1494.
[17] F. del Monte, M.P. Morales, D. Levy, A. Fernandez, M. Ocaña, A. Roig, E. Molins, K. O'Grady, C.J. Serna, Langmuir 13 (1997) 3627–3634.
[18] H.W. Kim, J.W. Lee, S.H. Shim, M.A. Kebede, C. Lee, Cryst. Res. Technol. 43 (2008) 695–699.
[19] R.K. Mishra, D.K. Pradhan, R.N.P. Choudhary, A. Banerjee, J. Phys.: Condens. Matter. 20 (2008) 045218.
[20] M. Mehring, Coord. Chem. Rev. 251 (2007) 974–1006.
[21] K. Matsumoto, K. Yamaguchi, T. Fujii, A. Ueno, J. Appl. Phys. 69 (1991) 5918–5920.
[22] S. Karimi, I.M. Reaney, Y. Han, J. Pokorny, I. Sterianou, J. Mater. Sci. 44 (2009) 5102–5112.
[23] J.-B. Li, G.H. Rao, Y. Xiao, J.K. Liang, J. Luo, G.Y. Liu, J.R. Chen, Acta Mater. 58 (2010) 3701–3708.
[24] A.A. Cristóbal, P.M. Botta, P.G. Bercoff, E.F. Aglietti, H.R. Bertorello, J.M. Porto López, J. Alloys Compd. 495 (2010) 516–519.
[25] Q. Yang, H. Zhang, L. Yingli, W. Qiye, IEEE Trans. Magn. 43 (2007) 3652–3655.
[26] Y.-P. Fu, C.-W. Cheng, D.-S. Hung, Y.-D. Yao, Ceram. Int. 35 (2009) 1509–1512.
[27] H. Zhao, J. Zhou, B. Li, Z. Gui, L. Li, J. Electroceram. 21 (2008) 802–804.
[28] M.S. Sverre, M.-A. Einarsrud, T. Grande, Chem. Mater. 21 (2009) 169–173.
[29] H. Namduri, S. Nasrazadani, Corros. Sci. 50 (2008) 2493–2497.
[30] P.B.A. Fechine, E.N. Silva, A.S. deMenezes, J. Derov, J.W. Stewart, A.J. Drehman, I.F. Vasconcelos, A.P. Ayala, L.P. Cardoso, A.S.B. Sombra, J. Phys. Chem. Solids 70 (2009) 202–209.
[31] V.L. Mathe, K.K. Patankar, J. Mater. Sci. 42 (2007) 136–142.
[32] E.M. Moreno, M. Zayat, M.P. Morales, C.J. Serna, A. Roig, D. Levy, Langmuir 18 (2002) 4972–4978.
[33] W. Wu, X.H. Xiao, S.F. Zhang, T.C. Peng, J. Zhou, F. Ren, C.Z. Jiang, Nanoscale Res. Lett. 5 (2010) 1474–1479.
[34] M.D. Mukadam, S.M. Yusuf, P. Sharma, S.K. Kulshreshtha, J. Magn. Magn. Mater. 272–276 (2004) 1401–1403.
[35] T.-J. Park, C.P. Georgia, J.V. Arthur, R.M. Arnold, S.W. Stanislaus, Nano Lett. 7 (2007) 766–772.